ARTICLE

Check for updates

Journal of
Sensor Science and Technology

The Korean Sensors Society

Microneedle Electrodes Preserve Long-Term EMG Stability against Stratum Corneum Remodeling

Gaeun Yun[1], Jungho Lee[1,2,+], Juhyeong Jeon[1], Phuong Thao Le[3], Hyeokjin Cho[1], Tae Sik Hwang[4,+], and Geunbae Lim[1,3,+]

[1]*Department of Mechanical Engineering, Pohang University of Science and Technology, Pohang, 37673, Republic of Korea*
[2]*Department of Emergency Medicine, College of Medicine, Chungnam National University, Daejeon, Republic of Korea*
[3]*Division of Interdisciplinary Bioscience and Bioengineering, Pohang University of Science and Technology, Pohang, 37673, Republic of Korea*
[4]*Department of Emergency Medicine, Sungkyunkwan University Samsung Changwon Hospital, Changwon, Republic of Korea*

Cite This: *J. Sens. Sci. Technol. Vol. 34, No. 6 (2025) 693-700*

https://doi.org/10.46670/JSST.2025.34.6.693

ABSTRACT: The stratum corneum (SC) presents a critical barrier for skin-mounted bioelectrodes, attenuating electrophysiological signals and limiting long-term stability. While transient improvements have been achieved with conformal film-based devices, their performance deteriorates over time, often attributed vaguely to interface degradation. Here we provide direct histological and quantitative evidence that continuous patch attachment induces progressive SC thickening, which substantially increases the electrode–skin barrier. Using controlled fabrication of film and microneedle (MN) electrodes on identical multilayer platforms, we demonstrate that both device types experience comparable SC remodeling, yet only film electrodes suffer from declining signal quality. In contrast, MN electrodes preserve intradermal channels within the thickened SC, maintaining stable contact with viable tissue and enabling high signal-to-noise ratio (SNR) electromyography (EMG) recordings over extended use. By linking dynamic SC remodeling to performance loss and visualizing how MN electrodes bypass this barrier, this work establishes a mechanistic basis for long-term reliable epidermal bioelectronics.

KEYWORDS: *Microneedle electrode, Stratum corneum remodeling, Electromyography (EMG), Signal stability, Wearable bioelectronics, Long-term stability*

1. INTRODUCTION

The stratum corneum (SC), the outermost layer of the skin, provides an essential barrier against the external environment but also imposes a critical challenge for epidermal bioelectronics. Because of its high electrical resistance and low ionic permeability, the SC significantly attenuates signal transmission between skin-mounted electrodes and the underlying tissues [1,2]. Conventional strategies to mitigate this barrier include conductive gels [3-6], skin preparation, and ultrathin-film-based epidermal electronics [7-14] that conform closely to the skin surface. Although such approaches improve initial coupling [15,16], they remain vulnerable to instability over time [17,18].

A key limitation is that the SC is not static; under continuous patch attachment, desquamation is suppressed, and corneocyte accumulation leads to progressive thickening. This remodeling process, although well recognized in dermatology, has rarely been documented in the context of bioelectrodes. As a result, long-term deterioration of signal quality is often ascribed generically to "interface degradation," without direct histological or quantitative evidence linking performance loss to SC dynamics.

Microneedle (MN) electrodes offer a promising solution as they physically penetrate the SC and establish direct electrical contact with the viable epidermis [19,20]. Previous reports have shown that MNs can reduce electrode–skin impedance and achieve high-quality biopotential recordings [21-25]. However, whether MN electrodes can sustain stable signal acquisition, specifically under conditions of SC remodeling, has not yet been systematically validated. In particular, direct

[+]Corresponding authors: double.arc@postech.ac.kr, emhwang1@hanmail.net, limmems@postech.ac.kr
Received : Oct. 16, 2025, Revised : Nov. 3, 2025, Accepted : Nov. 8, 2025

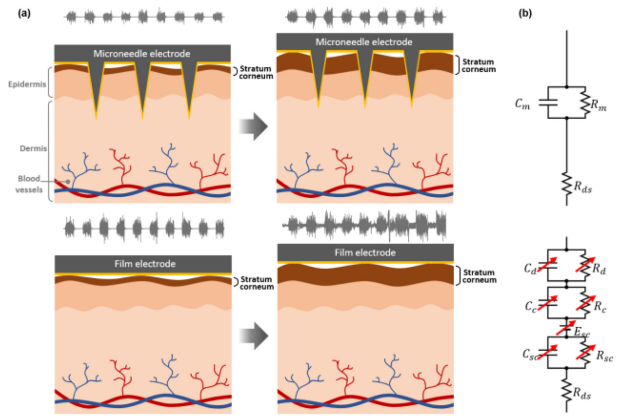

Fig. 1. Concept and equivalent circuit of microneedle electrodes. (a) Application of microneedle and film electrodes to the skin. While the microneedle electrode was unaffected by the increasing thickness of the stratum corneum over time, the film electrode exhibited a decrease in the signal-to-noise ratio (SNR) due to the thickening stratum corneum, which hindered signal measurement. (b) The electrical equivalent circuit models of the microneedle and film electrode system on skin.

evidence connecting occlusion-driven SC thickening to signal degradation in film electrodesand its circumvention by MN penetrationremains lacking.

Here, we address this gap by combining electrophysiological measurements with histological and quantitative analyses. We demonstrate that prolonged patch attachment induces significant SC thickening, which directly compromises the film electrode performance but not that of the MN electrodes. As shown in Fig. 1, the equivalent circuit analysis reveals that the SC adds a resistive–capacitive burden to the film electrodes, whereas the MN electrodes bypass this barrier. Correspondingly, electromyography (EMG) recordings illustrate that film electrodes suffer from declining signal-to-noise ratios (SNRs) as the SC thickens, whereas the MN electrodes preserve stable high-quality signals. Building on this conceptual framework, the subsequent sections provide experimental evidence spanning fabrication, mechanical and electrical characterization, histological validation, and in vivo recordings to establish the SC as the decisive factor in long-term electrode stability and to highlight the resilience of MN electrodes against this barrier.

2. METHODS

2.1 Electrode fabrication

Both film and microneedle (MN) electrodes were fabricated on flexible polyethylene terephthalate (PET, thickness 125 μm) substrates. A trilayer of parylene C (500 nm) / gold (100 nm) / parylene C (500 nm) was deposited using chemical vapor deposition (Parylene coater, Specialty Coating Systems) and e-beam evaporation (ZZS500, Maestech), followed by photolithographic patterning to define the electrode geometry. For the MN electrodes, arrays were replicated from SU-8 master molds using polydimethylsiloxane (PDMS, Sylgard 184, Dow Corning) and filled with an effervescent sacrificial matrix (polyvinylpyrrolidone, sodium bicarbonate, and citric acid). After curing, the parylene–Au–parylene film was laminated on top, and oxygen plasma etching (RIE-10NR, Samco) with a shadow mask selectively exposed the needle tips. PEDOT:PSS (Clevios PH1000, Heraeus) was electrodeposited on the tips (Gamry Reference 600 potentiostat) to reduce impedance and cured at 120°C for 1 h to improve adhesion and environmental stability. Film electrodes were fabricated using an identical parylene–Au–parylene process without MN integration, ensuring controlled comparison.

2.2 Mechanical characterization

Mechanical testing was performed using a universal testing machine (Instron 3343, 10 N load cell). Individual microneedles were compressed at a displacement rate of 0.04 mm/min to measure the fracture force (n = 10). The penetration force was evaluated on ex vivo porcine skin (thickness 1.5–2 mm) and the insertion depth was confirmed using optical coherence tomography (OCT; Thorlabs GANYMEDE). The average fracture force (~0.11 N/needle) exceeded the minimal force (~0.05 N/needle) required to penetrate the stratum corneum, ensuring robust insertion with a sufficient safety margin.

Each microneedle had a height of approximately 770 μm and a base diameter of 200 μm (aspect ratio ≈ 3.9), dimensions optimized to penetrate the stratum corneum without reaching deeper dermal structures.

2.3 Electrical characterization

Electrode resistance was measured using a source meter (Keithley 2400). Electrochemical impedance spectroscopy (EIS) was conducted in phosphate-buffered saline PBS (1×, pH 7.4) with a three-electrode configuration (Ag/AgCl reference, Pt mesh counter) at 10–100 kHz using a potentiostat (Gamry Reference 600). The PEDOT:PSS-coated electrodes exhibited reduced impedance at low frequencies compared to the uncoated controls, confirming the enhancement of electrode–tissue coupling. The conductive tip area of each microneedle was approximately 1.5×10^{-3} mm^2 (diameter ~44 μm), defined by selective oxygen plasma etching through a shadow mask and verified by optical microscopy.

2.4 Histological analysis

For histological evaluation, electrode sites were excised after application and fixed in 10% neutral buffered formalin for 24 h. Samples were paraffin-embedded, sectioned at 5 μm thickness, and stained with hematoxylin and eosin (H&E). Images were captured using an optical microscope (Olympus BX53) and analyzed using ImageJ software. Stratum corneum (SC) thickness was quantified from at least five randomly selected regions per sample (n = 3 per condition).

2.5 In vivo EMG recordings

Human EMG experiments were approved by the Institutional Review Board (IRB, CNUH-2023-09-001) and performed on healthy adult volunteers (n = 5). The electrodes were placed on the forearm flexor muscles with an inter-electrode spacing of 20 mm. Signals were recorded using a biopotential amplifier (NI USB-6343, National Instruments) at a sampling rate of 2 kHz with bandpass filtering (20–500 Hz) and a 60 Hz notch filter. The subjects performed repeated cycles of hand clenching and relaxation. Signal-to-noise ratio (SNR) was calculated as the ratio of the RMS signal amplitude during contraction to the baseline noise RMS. The long-term stability was assessed by repeated measurements on days 1 and 3 under identical placement conditions.

2.6 Statistical analysis

All data are presented as mean ± standard deviation. Statistical significance was evaluated using paired t-tests or one-way analysis of variance (ANOVA) with Tukey's post hoc tests, as appropriate, with a significance level of $p < 0.05$.

3. RESULTS AND DISCUSSIONS

The concept illustrated in Fig. 1 was validated using direct signal measurements. Although both the film and MN electrodes initially recorded comparable EMG activity, only the MN electrodes maintained high-quality waveforms over time (Fig. 1(a)). In contrast, the film electrodes exhibited a progressive degradation of the SNR as the SC thickened, which was consistent with the equivalent circuit interpretation (Fig. 1(b)). These results confirm that the superior long-term performance of MN electrodes originates from their ability to bypass the SC barrier and preserve stable electrode–skin coupling.

To enable a controlled comparison, both electrode types were fabricated using an identical platform consisting of a parylene–Au–parylene stack patterned on PET substrates, with

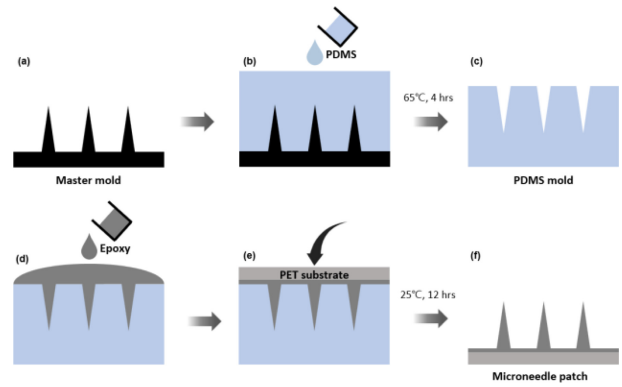

Fig. 2. Microneedle patch fabrication process. (a) Fabrication of microneedle master mold using grayscale lithography. (b) Casting of PDMS to form negative replica of master mold. (c) Curing of PDMS inverse mold at 65°C for 4 h. (d) Pouring of medical epoxy into mold. (e) Lamination of PET substrate onto epoxy, followed by vacuum filling of medical epoxy into needle tip and curing at 25°C for 12 h. (f) Fabricated microneedle patch.

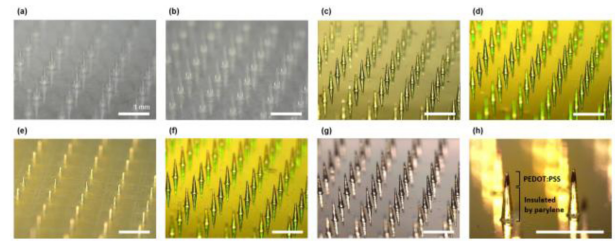

Fig. 3. The sequential fabrication steps of microneedle electrodes. (a) Replication of epoxy microneedle patch via soft lithography. (b) Deposition of 500 nm parylene layer onto microneedle patch. (c) Deposition of gold layer to form conductive electrode. (d) Deposition of 500 nm parylene insulating layer. (e) Application of shadow mask to microneedle tips. (f) Etching of parylene layer at tips by oxygen plasma. (g) Electrodeposition of PEDOT:PSS onto microneedle tips. (h) inal fabricated microneedles. All scale bars, 1 mm.

the sole distinction being the presence or absence of microneedle arrays. The detailed fabrication scheme is shown in Figs. 2 and 3.

To create microneedle (MN) scaffolds with controlled geometry, we first prepared grayscale-lithography master molds, replicated them in PDMS, and cast medical epoxy into the negative molds. After laminating a PET backing and curing (65°C, 4 h; then 25°C, 12 h), complete epoxy MN patches were obtained (Fig. 2). These patches served as the structural basis for the subsequent electrode integration.

Both the film and MN devices were built on the same parylene–Au–parylene stack. For the MN electrodes, the multilayers were conformally coated onto the epoxy needles, and a shadow mask and oxygen plasma exposed only the apex to act as the working contact, while the shaft remained

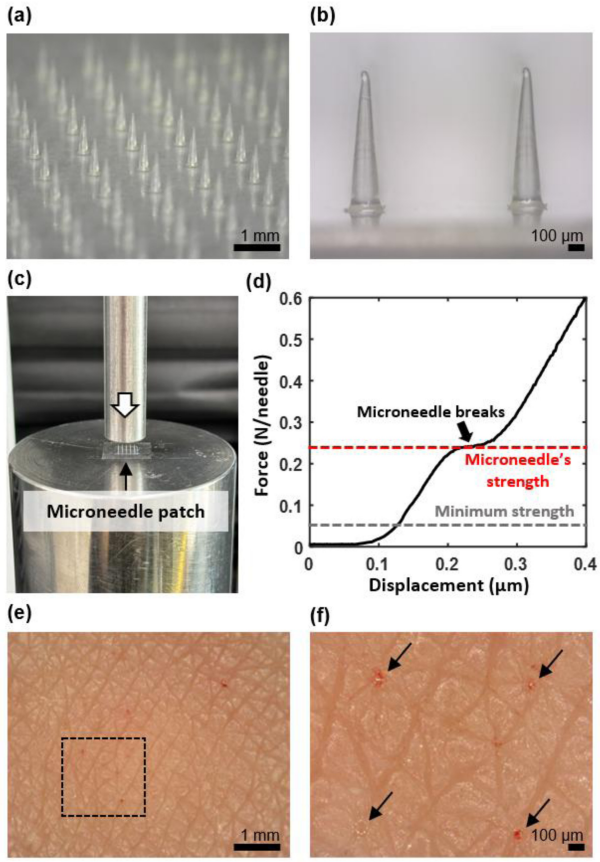

Fig. 4. Characterization of microneedle array structure and mechanical performance. (a) Optical microscopy image of microneedle array and (b) detailed view of individual microneedles. (c) The experimental setup for measuring the fracture force of the microneedles. (d) Force and frequency curve obtained during the compression test of a microneedle, demonstrating its mechanical strength. (e) Microscopic image of the surface of the human skin after the microneedles penetration. (f) Higher-magnification image showing micropores created by microneedles; arrows indicate micropores.

insulated. PEDOT:PSS was finally deposited on the exposed tips to lower low-frequency impedance. The film electrodes were subjected to identical metallization/encapsulation steps on flat PET, ensuring that the sole variable was MN penetration (Fig. 3).

The mechanical robustness of the microneedle arrays was evaluated to ensure reliable skin penetration without structural failures (Fig. 4). Compression tests demonstrated that the individual microneedles withstood forces exceeding the minimum insertion threshold, confirming a sufficient safety margin for consistent penetration. The measured fracture force was several times higher than the estimated force required to breach the stratum corneum, indicating that the microneedles were mechanically stable under typical handling and

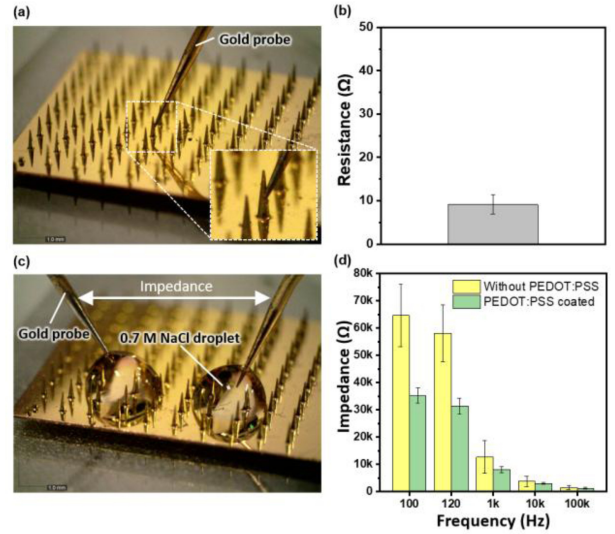

Fig. 5. Electrical properties of microneedle electrodes. (a) Setup for measuring the resistance between the microneedle and the electrode wire and (b) the measured resistance. (c) Setup for impedance measurements of the microneedle electrodes and (d) the impedance spectra of the microneedle electrodes before and after PEDOT:PSS coating.

application conditions.

In parallel, penetration tests on the excised skin confirmed reproducible insertion with minimal deformation of the surrounding tissue. The microneedles created consistent microchannels that were maintained across repeated applications, thereby demonstrating the mechanical reliability of the array design. Importantly, no structural collapse or tip blunting was observed after multiple uses, supporting the durability of the parylene–Au–parylene coating during penetration.

These results establish that microneedles provide a mechanically robust yet minimally invasive interface capable of reproducible insertion into the skin barrier, while preserving structural integrity for long-term use.

The intrinsic electrical properties of the electrodes were characterized to confirm that the performance differences arose from the electrode–skin interface rather than the electrodes themselves (Fig. 5). Measurements of line resistance and contact resistance revealed values in the range of a few tens of ohms, with no significant differences between film and MN electrodes. This indicates that the conductive parylene-Au-parylene layers maintained stable electrical continuity, independent of the device configuration.

Electrochemical impedance spectroscopy (EIS) further demonstrated comparable characteristics when the electrodes were immersed in a saline environment. Both electrode types exhibited similar impedance spectra across the frequency range, confirming that the electrode materials and

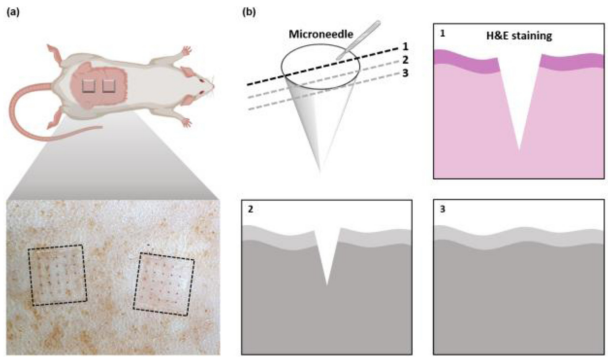

Fig. 6. Preparation of skin sections for histological analysis of microneedle electrode sites. (a) Microneedle patches applied to the dorsal skin of a Sprague-Dawley (SD) rat. (b) Schematic representation of the cross-sectional views of rat skin at various locations. The sections were prepared by cutting the skin at various positions relative to the microneedle, including the exact center of the microneedle. The central section was then stained with Hematoxylin & Eosin (H&E) to visualize tissue morphology.

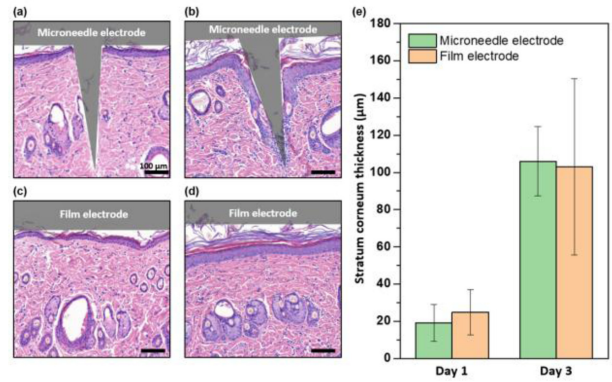

Fig. 7. Histopathological analysis of SD rat skin in vivo after microneedle and film electrodes application. Microscopic images of hematoxylin and eosin (H&E)-stained tissue sections of rat skin (a) immediately after and (b) 2 days after microneedle electrode application, and (c) immediately after and (d) 2 days after film electrode application. Scale bar showing 100μm. (e) Measurement of stratum corneum thickness based on obtained images.

encapsulation provided equivalent intrinsic performances. The incorporation of conductive surface treatments, such as PEDOT:PSS coating, further reduced the low-frequency impedance but did not alter the relative equivalence between the film and the MN electrodes.

Together, these measurements established that the observed differences in the long-term biosignal quality cannot be attributed to variations in the electrode material or baseline electrical properties. Instead, the results highlighted the role of the SC barrier as the dominant factor in interface impedance during skin application, thereby isolating microneedle penetration as the key determinant of improved SNR in subsequent in vivo experiments.

To investigate how prolonged electrode attachment alters the skin barrier, histological sections were prepared from microneedle (MN) electrode sites and examined by hematoxylin and eosin (H&E) staining (Fig. 6). To ensure an accurate evaluation of the tissue response, the skin was sectioned along different planes relative to the microneedles, including the exact central axis of the needle shafts. Sectioning through the needle axis allowed direct visualization of the penetration depth and tissue interactions, providing a fair comparison across samples. On day 1, the SC appeared relatively thin and uniform, whereas on day 3, a clear thickening of the SC was observed under occlusive attachment. Beyond three days, no significant change in SC thickness was observed; and therefore three days was taken as the long-term condition for this study, and similar outcomes are expected for longer durations. Importantly, at the MN electrode sites, the microchannels created by needle insertion remained visible across the thickened SC, whereas deeper epidermal and dermal structures remained intact, confirming that penetration was confined to the barrier layer without tissue disruption.

To quantify the effect of occlusion on the SC, we performed histological analysis of skin samples collected from animal models after repeated electrode attachment (Fig. 7). Hematoxylin and eosin (H&E)-stained sections were prepared along the microneedle axis, and the SC thickness was measured across multiple regions for consistent evaluation. Quantitative analysis confirmed that the SC thickness increased significantly from day 1 to day 3, regardless of whether film or MN electrodes were applied. This indicated that patch occlusion itself promoted corneocyte accumulation and barrier thickening. Although SC thickening is primarily driven by inhibited desquamation under occlusion, other secondary factors such as limited sweat drainage or mild local immune responses may further influence the remodeling process.

Importantly, despite this comparable increase in SC thickness, the MN electrodes maintained their conductive tips exposed in the upper dermis through the microchannels created by penetration. Thus, even as the SC thickened, the electrode–tissue interface of the MN devices remained functionally preserved, whereas the film electrodes were entirely subjected to the reinforced barrier. These results provide direct histological evidence that the divergence in long-term signal quality between MN and film electrodes arises not from differences in SC remodeling but from whether the electrode can bypass the thickened layer.

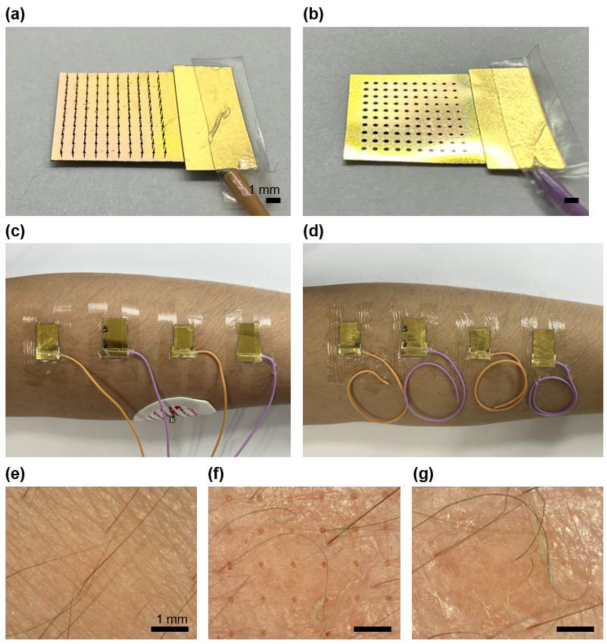

Fig. 8. Experimental setup for EMG signal monitoring. (a) Microneedle electrodes and (b) film electrodes for EMG signal monitoring. (c) Right after applying the microneedle and film electrodes to a human forearm and (d) after 2 days of application. Microscopic images of (e) skin without electrode application, (f) skin with microneedle and (g) film electrode application after 2 days.

To further validate these histological findings in the human skin, we examined occlusion-induced changes directly at the electrode application sites. As shown in Fig. 8, both the film and MN patches promoted SC thickening after several days of wear; however, only the MN electrodes preserved the intradermal conduits, maintaining connectivity to viable tissue despite the thickened barrier.

Next, we evaluated the performances of the film and MN electrodes in human subjects to confirm their applicability to real-time EMG monitoring (Fig. 8). Both electrode types were fabricated on the same parylene-Au-parylene platform and placed on the forearm flexor muscles in identical configurations. At the initial time point (day 1), both the film and MN electrodes successfully captured EMG signals with comparable waveform quality, indicating that the baseline coupling was effective regardless of the electrode type. Visual inspection of the electrode sites revealed no irritation or erythema, confirming the short-term biocompatibility. Notably, at the MN electrode sites, microscopic examination revealed the presence of minimal microchannels corresponding to needle penetration, whereas the surrounding skin remained intact. In contrast, film electrode sites exhibited accumulation of desquamating corneocytes after two days of occlusive attachment, consistent with the barrier remodeling observed in

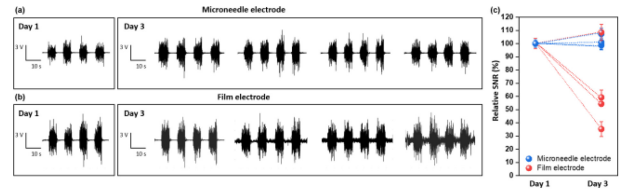

Fig. 9. EMG signals from human subject via MN vs film electrodes. The EMG signals obtained from (a) microneedle electrodes and (b) film electrodes immediately after application (Day 1) and after 2 days (Day 3). (c) Relative signal-to-noise ratio (SNR) values for day 1 and day 3.

histological analysis. These results demonstrate that both electrode types are capable of safe and effective initial recordings; however, the MN interface provides a more stable pathway for long-term measurements by mitigating the effects of SC buildup.

Finally, we compared the long-term stability of EMG recordings obtained with film and MN electrodes over three days of continuous use (Fig. 9). On day 1, both electrode types recorded muscle activity with similar waveform amplitudes and clarity. By day 3, however, the film electrodes exhibited pronounced signal degradation with reduced amplitude and distorted waveforms, consistent with the increase in impedance caused by SC thickening. In contrast, the MN electrodes maintained waveforms with stable amplitudes and temporal features, demonstrating their resilience to barrier changes. Quantitative analysis of the signal-to-noise ratio (SNR) confirmed this divergence: film electrodes showed a substantial decline in the relative SNR, whereas MN electrodes retained nearly constant values throughout the measurement period. These findings directly validate the concept illustrated in Fig. 1, establishing that bypassing the SC barrier is a decisive factor for preserving high-fidelity EMG signals during long-term monitoring.

4. CONCLUSIONS

In this study, we provided direct evidence that continuous on-skin attachment remodels the stratum corneum (SC), producing progressive thickening that directly undermines performance of film-based electrodes. By combining histological visualization and quantitative analysis with in vivo EMG measurements, we demonstrated that barrier remodeling is the primary driver of long-term signal degradation in conventional epidermal electrodes.

Microneedle (MN) electrodes circumvent this barrier by penetrating the SC and maintaining stable intradermal channels, even after significant thickening. As a result, MN electrodes preserve a high signal-to-noise ratio (SNR) and

waveform fidelity throughout extended EMG monitoring, in stark contrast to the decline observed with film electrodes.

These findings not only validate MN electrodes as a robust platform for reliable, long-term epidermal bioelectronics but also establish SC remodeling as a key mechanistic bottleneck for skin-mounted devices. Recognizing and addressing these dynamic barriers is essential for designing next-generation wearable clinical monitoring technologies. Future studies should also explore breathable or porous electrode architectures that can reduce occlusion-induced SC thickening by allowing limited vapor and sweat exchange, thus providing an alternative route to improve long-term skin compatibility.

CRediT Authorship Contribution Statement

Gaeun Yun: Conceptualization, Data curation, formal analysis, Investigation, Methodology, Validation, Visualization, Writing the original draft. **Jungho Lee:** Supervision, Investigation, Funding acquisition. **Juhyeong Jeon:** Investigation. **Phuong Thao Le:** Investigation. **Hyeok Jin Cho:** Investigation. **Tae Sik Hwang:** Supervision, Funding acquisition. **Geunbae Lim:** Supervision, Funding acquisition.

Declaration of Competing Interest

The authors declare that they have no known competing financial interests or personal relationships that could have appeared to influence the work reported in this paper.

Acknowledgements

This study was supported by a faculty research grant from the Yonsei University College of Medicine (6-2023-0087) and the Basic Science Research Program through the National Research Foundation of Korea (NRF), funded by the Ministry of Education (RS-2024-00452785).

REFERENCES

[1] L. Kalevo, T. Miettinen, A. Leino, S. Kainulainen, H. Korkalainen, K. Myllymaa, et al., Effect of sweating on electrode-skin contact impedances and artifacts in EEG recordings with various screen-printed Ag/AgCl electrodes, IEEE Access 8 (2020) 50934–50943.

[2] L.M. Ferrari, U. Ismailov, J.-M. Badier, F. Greco, E. Ismailova, Conducting polymer tattoo electrodes in clinical electro- and magneto-encephalography, npj Flex. Electron. 4 (2020) 4.

[3] S. Choi, S.I. Han, D. Jung, H.J. Hwang, C. Lim, S. Bae, et al., Highly conductive, stretchable and biocompatible Ag–Au core–sheath nanowire composite for wearable and implantable bioelectronics, Nat. Nanotechnol. 13 (2018) 1048–1056.

[4] C. Zhao, J. Park, S.E. Root, Z. Bao, Skin-inspired soft bioelectronic materials, devices and systems, Nat. Rev. Bioeng. 2 (2024) 671–690.

[5] J. Deng, H. Yuk, J. Wu, C.E. Varela, X. Chen, E.T. Roche, et al., Electrical bioadhesive interface for bioelectronics, Nat. Mater. 20 (2021) 229–236.

[6] J.-Y. Sun, C. Keplinger, G. Whitesides, Z. Suo, Ionic skin, Adv. Mater. 26 (2014) 7608–7614.

[7] D.-H. Kim, N. Lu, R. Ma, Y.-S. Kim, R.-H. Kim, S. Wang, et al., Epidermal electronics, Science 333 (2011) 838–843.

[8] T. Someya, M. Amagai, Toward a new generation of smart skins, Nat. Biotechnol. 37 (2019) 382–388.

[9] T. Someya, T. Sekitani, S. Iba, Y. Kato, H. Kawaguchi, T. Sakurai, A large-area, flexible pressure sensor matrix with organic field-effect transistors for artificial skin applications, Proc. Natl. Acad. Sci. 101 (2004) 9966–9970.

[10] T. Someya, Y. Kato, T. Sekitani, S. Iba, Y. Noguchi, Y. Murase, et al., Conformable, flexible, large-area networks of pressure and thermal sensors with organic transistor active matrixes, Proc. Natl Acad. Sci. 102 (2005) 12321–12325.

[11] J.Y. Oh, S. Rondeau-Gagné, Y.-C. Chiu, A. Chortos, F. Lissel, G.-J.N. Wang, et al., Intrinsically stretchable and healable semiconducting polymer for organic transistors, Nature 539 (2016) 411–415.

[12] T. Sekitani, Y. Noguchi, K. Hata, T. Fukushima, T. Aida, T. Someya, A rubberlike stretchable active matrix using elastic conductors, Science 321 (2008) 1468–1472.

[13] A. Miyamoto, S. Lee, N.F. Cooray, S. Lee, M. Mori, N. Matsuhisa, et al., Inflammation-free, gas-permeable, lightweight, stretchable on-skin electronics with nanomeshes, Nat. Nanotechnol. 12 (2017) 907–913.

[14] S. Lee, S. Franklin, F.A. Hassani, T. Yokota, M.O.G. Nayeem, Y. Wang, et al., Nanomesh pressure sensor for monitoring finger manipulation without sensory interference, Science 370 (2020) 966–970.

[15] F. Ershad, A. Thukral, J. Yue, P. Comeaux, Y. Lu, H. Shim, et al., Ultra-conformal drawn-on-skin electronics for multifunctional motion artifact-free sensing and point-of-care treatment, Nat. Commun. 11 (2020) 3823.

[16] Z. Liu, X. Xu, S. Huang, X. Huang, Z. Liu, C. Yao, et al., Multichannel microneedle dry electrode patches for minimally invasive transdermal recording of electrophysiological signals, Microsyst. Nanoeng. 10 (2024) 72.

[17] J. Heikenfeld, A. Jajack, J. Rogers, P. Gutruf, L. Tian, T. Pan, et al., Wearable sensors: modalities, challenges, and prospects, Lab Chip 18 (2018) 217–248.

[18] Y. Hou, Z. Li, Z. Wang, H. Yu, Miura-ori structured flexible microneedle array electrode for biosignal recording, Microsyst. Nanoeng. 7 (2021) 53.

[19] X. Tang, Y. Dong, Q. Li, Z. Liu, N. Yan, Y. Li, et al., Using microneedle array electrodes for non-invasive electrophysiological signal acquisition and sensory feedback evoking, Front. Bioeng. Biotechnol. 11 (2023) 1238210.

[20] H. Ji, M. Wang, Y. Wang, Z. Wang, Y. Ma, L. Liu, et al., Skin-integrated, biocompatible, and stretchable silicon microneedle electrode for long-term EMG monitoring in motion scenario, npj Flex. Electron. 7 (2023) 46.

[21] H. Lee, T.K. Choi, Y.B. Lee, H.R. Cho, R. Ghaffari, L. Wang, et al., A A graphene-based electrochemical device with thermoresponsive microneedles for diabetes monitoring and therapy, Nat. Nanotechnol. 11 (2016) 566–572.
[22] W. Lee, S.-H. Jeong, Y.-W. Lim, H. Lee, J. Kang, H. Lee, et al., Conformable microneedle pH sensors via the integration of two different siloxane polymers for mapping peripheral artery disease, Sci. Adv. 7 (2021) eabi6290.
[23] Q. Zhao, E. Gribkova, Y. Shen, J. Cui, N. Naughton, L. Liu, et al., Highly stretchable and customizable microneedle electrode arrays for intramuscular electromyography, Sci. Adv. 10 (2024) eadn7202.
[24] D. Yan, A.A. Jiman, E.C. Bottorff, P.R. Patel, D. Meli, E.J. Welle, et al., Ultraflexible and stretchable intrafascicular peripheral nerve recording device with axon-dimension, cuff-less microneedle electrode array, Small 18 (2022) e2200311.
[25] H. Kim, J. Lee, U. Heo, D.K. Jayashankar, K.-C. Agno, Y. Kim, et al., Skin preparation–free, stretchable microneedle adhesive patches for reliable electrophysiological sensing and exoskeleton robot control, Sci. Adv. 10 (2024) eadk5260.